Nano Res
DOI 10.1007/s12274-012-0267-5
Research Article

Repair and Stabilization in Confined Nanoscale Systems - Inorganic Nanowires within Single-Walled Carbon Nanotubes

Adelina Ilie[1](✉), Simon Crampin[1], Lisa Karlsson[2] and Mark Wilson[3]

[1] Department of Physics & Centre for Graphene Science, University of Bath, Bath, BA2 7AY, United Kingdom
[2] Department of Materials, University of Oxford, Oxford, OX1 3PH, United Kingdom
[3] Department of Chemistry, Physical and Theoretical Chemistry Laboratory, University of Oxford, Oxford, OX1 3QZ, United Kingdom

Received: day month year / Revised: day month year / Accepted: day month year (automatically inserted by the publisher)

ABSTRACT

Repair is ubiquitous in biological systems, but rare in the inorganic world. We show that inorganic nanoscale systems can however possess remarkable repair and reconfiguring capabilities when subjected to extreme confinement. Confined crystallization inside single-walled carbon nanotube (SWCNT) templates is known to produce the narrowest inorganic nanowires, but little is known about the potential for repair of such nanowires once crystallized, and what can drive it. Here inorganic nanowires encapsulated within SWCNTs were seen by high-resolution transmission electron microscopy to adjust to changes in their nanotube template through atomic rearrangement at room temperature. These observations highlight nanowire repair processes, supported by theoretical modeling, that are consistent with atomic migration at fractured, ionic ends of the nanowires encouraged by long-range force fields, as well as release-blocking mechanisms where nanowire atoms bind to nanotube walls to stabilize the ruptured nanotube and allow the nanowire to reform. Such principles can inform the design of nanoscale systems with enhanced resilience.

KEYWORDS

Filled Carbon Nanotubes, Nanowires, Repair, HRTEM, Density Functional Theory, Molecular Dynamics

1. Introduction

A desirable attribute for robust nanoscale systems is an ability to repair after damage, so that understanding what can drive repair is a critical aspect of system design. Though a staple feature of bio-related systems, repair is otherwise rare, but here we show that inorganic systems can also possess remarkable capabilities to repair and reconfigure when subjected to extreme confining environments. We study inorganic nanowires encapsulated inside single-walled carbon nanotubes (SWCNTs), which reveal reconfiguring dynamic phenomena involving both filling and nanotube that promote nanowire repair.

SWCNT templating uniquely produces very narrow,

atomically regulated nanowires, that would not be stable and form otherwise [1], and have unique prospects in chemical sensing, electron and spin transport, nanoscale mass-transport or drug delivery [2]. The most regularly used technological route to this end is crystallization from molten phase [1], where molten filling material penetrates the confining environment of the inner cavity of the nanotube through its open ends or side-wall defects and subsequently crystallizes. The processes leading to nanowire formation are well on their way to being fully understood [3], however an interesting question is whether the same interactions can act towards nanowire repair or reconfiguration following structural damage even when the nanowire is already crystallized. The reconstructive behaviour of such confined nanowires, to what extent repair can occur, and what mechanisms can drive repair are virtually unstudied.

When nanotubes are filled, the inner surface of the nanotube template can engage in chemical reactions and dynamic processes initiated or catalysed by the filling [4]. Such phenomena involve not only oxygen containing compounds [5], but are more general and whether they occur or not depends on the bonding energy of the filling species with the nanotube inner wall [6]. In this context, it is not unreasonable to expect some interplay between the structural evolutions of the inner nanowire and the nanotube sheath, manifesting in both destructive and restorative processes. In the case of empty SWCNTs, self-repair of large (20 atom-) multivacancies has been claimed at room temperature [7], challenging current theories and other reports that favour the repair of only much smaller holes [8-11] and that require substantial thermal energy [10]. More generally, the ability of the nanotube wall to reconfigure (irrespective whether considered as "self-repair" or rather being electron beam-assisted) and eliminate larger holes favours the repair of the encapsulated nanowires as filling species permeate the nanotube only when the size of its multivacancies exceed a certain threshold. Here we exploited structural changes in the nanotube to provide a situation for the nanowire to evolve and reconfigure.

In this work we induced ejection of sub-units of nanowires from within SWCNTs under electron-beam exposure and observed subsequent processes of repair. We found initial defect creation in the nanotube wall did not lead to major disruption of either nanotube or encapsulated nanowire, but triggered competing dynamic phenomena of ejection, motion and repair. The systems we studied, encapsulated inorganic nanowires of silver iodide (AgI) and iodine (I), governed by ionic/polarization and van der Waals interactions respectively, allowed us to uncover different scenarios that favour nanowire repair. In medium-sized SWCNTs (~1.4 nm diameter), sufficiently deformable AgI crystals were observed to repair through atomic/bond rearrangement driven to conform to the new environment, highlighting a pathway towards a more general mechanism for nanowire repair, and also involving long-range electrostatic forces. Very narrow SWCNTs (<1.1 nm diameter) filled with iodine ribbons, and expected to have little structural stability [12], were able to sustain repeated sequential events of atom ejection and healing or blocking of the wall defects, while the iodine structure inside underwent repair. These results demonstrate remarkable capabilities that nanostructures can possess to repair and reconfigure when subjected to extreme confining environments.

We used the molten phase technique to produce crystalline AgI nanowires inside SWCNTs (AgI@SWCNTs) according to established procedures and our previous work [2, 13]. Extensive studies [2] have revealed various encapsulated AgI structures, dependent upon the nanotube diameter and stemming from the well-known bulk AgI polymorphism with subsequent relaxation inside the nanotube. Iodine nanowires can also form very occasionally, as found here, as a by-product of AgI dissociation in the surrounding medium; their distinctive diameter-dependent phases have been established in Ref. [14]. We used High Resolution Transmission Electron Microscopy (HRTEM) to resolve the initial structure of encapsulated AgI and I nanowires and record their subsequent evolution under increased electron beam doses. We used an accelerating voltage of 100 kV, which is above the knock-on threshold of carbon atoms from both empty [15] and filled carbon nanotubes [4], in order to create ejection sites in the nanotube wall, but kept the doses orders of magnitude lower (in the range 0.4

to 2 A/cm^2) than values used in other works [16], in order to delay and reduce carbon knock-on damage [9, 17] as well as slow down the frequency of the events occurring within the encapsulated nanowires while capturing those in real time (see Methods). Working at sub-threshold energy, where the nanotube cage remains intact, would not offer the same opportunities for nanowire evolution (see Methods). Complementary density functional theory (DFT) and molecular dynamics (MD) studies (see Methods) were used to support the dynamic processes and structural configurations we proposed.

2. Results

Panel 1 of Figure 1(a) shows a HRTEM image of an AgI@SWCNT (in 1.4 nm diameter nanotube), observed over ~ 10 nm before continuing over a longer length under obstructing material residing in a different plane (see Electronic Supplementary Material ESM-1). AgI filling was confirmed by Energy Dispersive X-ray spectroscopy (EDX) on similar structures, an example of which is shown in ESM-1. Image in panel 1 and associated sets of focal series and exit wavefunction reconstruction images (see Methods and ESM-1) are compatible with a relaxed structure of bulk AgI (Figure 1(b), (c-d), and ESM-1). DFT calculations showed that, persistently, silver atoms relax towards the interior of the structure, reducing ionicity of outer atoms. There is virtually no bonding of this structure with the nanotube wall (as shown by the centred structure and clear van der Waals spacing to the wall, and supported by DFT calculations yielding negligible electron transfer between nanotube and nanowire). This permits occasional rotation of the structure between orientations p1 and p2 (Figure 1(c),(d)) yielding two different sets of focal series (to which Figure 1(a) Panels 1-4, and 5-9 belong, respectively; see ESM-1).

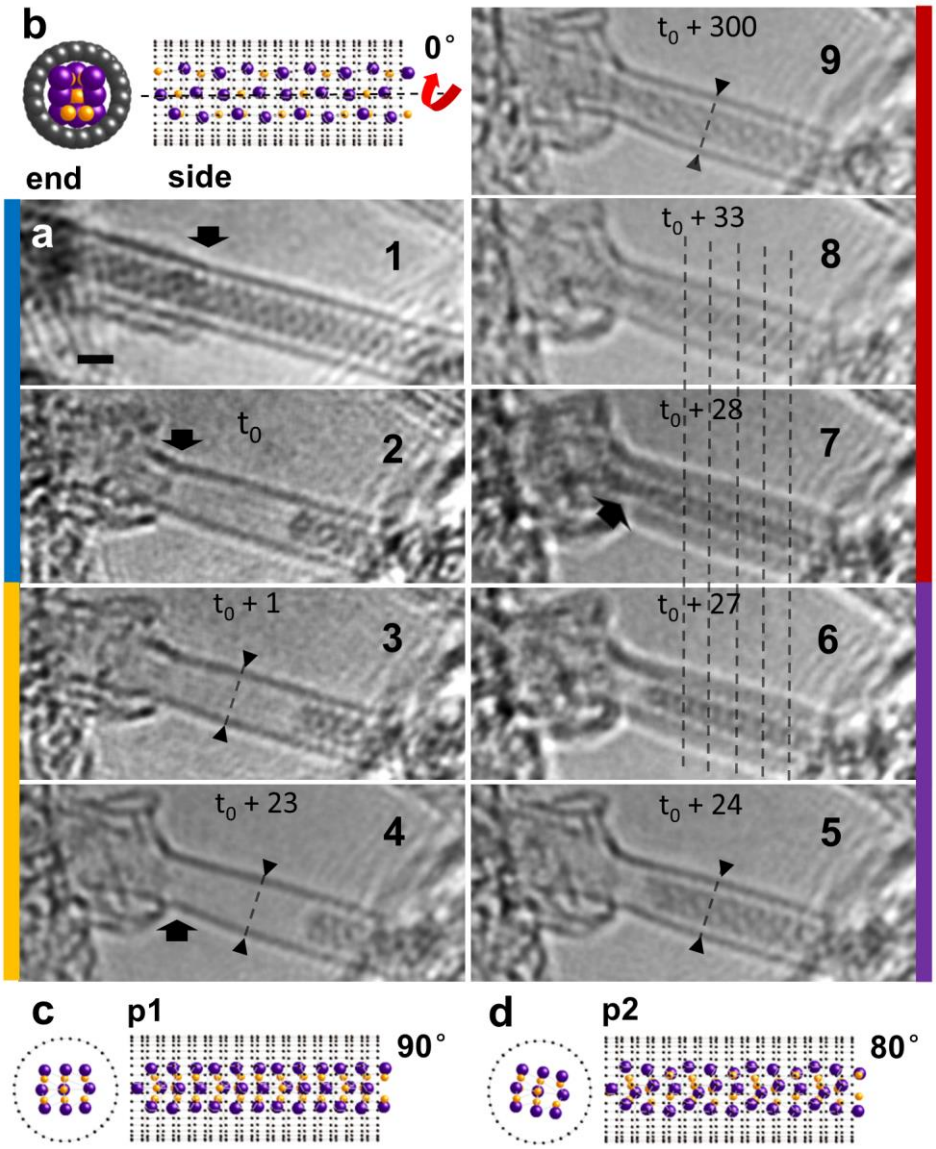

Figure 1 Key evolutionary stages of AgI@SWCNT nanowire: ejection, motion and subsequent repair. (a) HRTEM images at different focal distances that link to four stages described in main text, signposted by side colour bars. Relative time sequence is shown in seconds. Panel 1 shows the structure before evolution. Large arrows point to key events, such as the nanotube kinks and constriction in Panels 1,2 and 4, and material diffusion through nanotube constriction in Panel 7. Dashed lines with small arrows delimit the end of the "funnel" region in which the nanotube reconstructs after the initial kink in Panel 2. Panels 5 and 9 demonstrate that the AgI structure at the right side of the constriction is preserved during stage 4 of nanowire repair. The original AgI structure is preserved in the undeformed region of the tube at right, while "shearing" occurs at the end penetrating the funnel region. (b) Proposed structural model of the AgI nanowire inside the un-deformed nanotube (obtained by relaxing a bulk zincblende cut with the [-1,-1,2] direction along the long axis). Rotating this structure around its long axis leads to structures in (c): p1 (90° rotation) and p2 (80° rotation), corresponding to Panels 1-4, and 5-9 in (a), respectively. Images are part of focal series (shown in ESM-1).

Panels 1 – 9 in Figure 1(a) capture several key evolutionary stages of this AgI@SWCNT structure under irradiation at a fixed electron beam dose of 2 A/cm^2. Prior to this, imaging at lower doses (0.4 to 1 A/cm^2) for tens of minutes caused no visible changes to the nanotube or encapsulated nanowire, and only little and very gradual e-beam induced contamination of the adjacent regions. Then, in Stage 1 (Panels 1-2), a kink, visible in the upper left side of the nanotube wall in Panel 1, evolves to become

much more pronounced in Panel 2. Concomitantly, material is released, with kinetics that are fast enough for the release of the filling to not be captured in successive images (taken every 1s), with Panels 2 and 3 showing successive images just after ejection of a few nm long AgI section. We identified the kink as the likely ejection site (as opposed to, potentially, ends of the nanotube located beyond the imaged region) based on the fact that the only region in the exposed area that showed significant build-up of material, suddenly and *concomitant* with the enlargement of the kink is the one located immediately adjacent to its left (see larger area in ESM-1). This suggests that vacancies sufficiently large to allow AgI sublimation were created in the nanotube in the first instance.

A strong contrast fragment is seen in Panel 2 in the region of the kink, then not visible any longer in Panel 3. Previously [18], in the release of copper iodide (CuI) from Multi-Walled Carbon Nanotubes, I^- ions were identified as the first to be ejected, leaving behind the metal cations. This scenario is also consistent with the side-wall mechanism proposed in Ref. [16] where halogen release converts encapsulated silver halides into Ag inside damaged SWCNTs. In Stage 2 (Panels 3-4), a funnel-like constriction, 3.5 nm long, evolves from the upper kink along the nanotube reaching a stable, reconstructed configuration as in Panel 4. The funnel reaches 1.1 nm (a 25% reduction) in diameter at its narrowest. In Stage 3 (Panel 5), the right side of the AgI crystal migrates part-way inside the constriction – again a rapid process occurring below the 1 s time resolution - and conforms to the shrinking diameter of that region while the van der Waals gaps remain clear, indicating negligible bonding with the nanotube wall. Importantly, no further sublimation occurs during this stage or later, over many minutes of exposure. In Stage 4 (Panel 7), material enters from the left side through the constriction to join the AgI crystal on the right side. This effects a repair through the neck region of the AgI nanowire, which is reconstituted as a continuous structure. This repair is not accomplished by the migration of AgI material from the right hand side, as evidenced by the constancy throughout Panels 6-8 of the number and position of motifs in that area (dashed lines in panels 6-8). Panels 8-9 show the final AgI nanowire at two further focal distances.

The evolution described above highlights two critical aspects that determine stability and repair in these hybrid systems. Firstly, what changes to the vacancy in the nanotube wall occur that stop further permeation through the wall and hence sublimation? Secondly, what processes drive two disjoint parts of a nanowire to reconnect and repair? Concerning the former, here, iodine is the largest species involved in sublimation, and we use it as a probe of the size of side-wall vacancies. A second dynamic process that we observed, Figure 2, where iodine is sequentially released, over tens of minutes, through the side of a 1.1 nm diameter nanotube containing a two-atomic row iodine nanoribbon, suggests a possible "plugging" mechanism. Several ejection / reorganization events were captured as an example in a movie that covered 40 s in real time (available as ESM-2). This movie was also used to generate Figure 2(c).

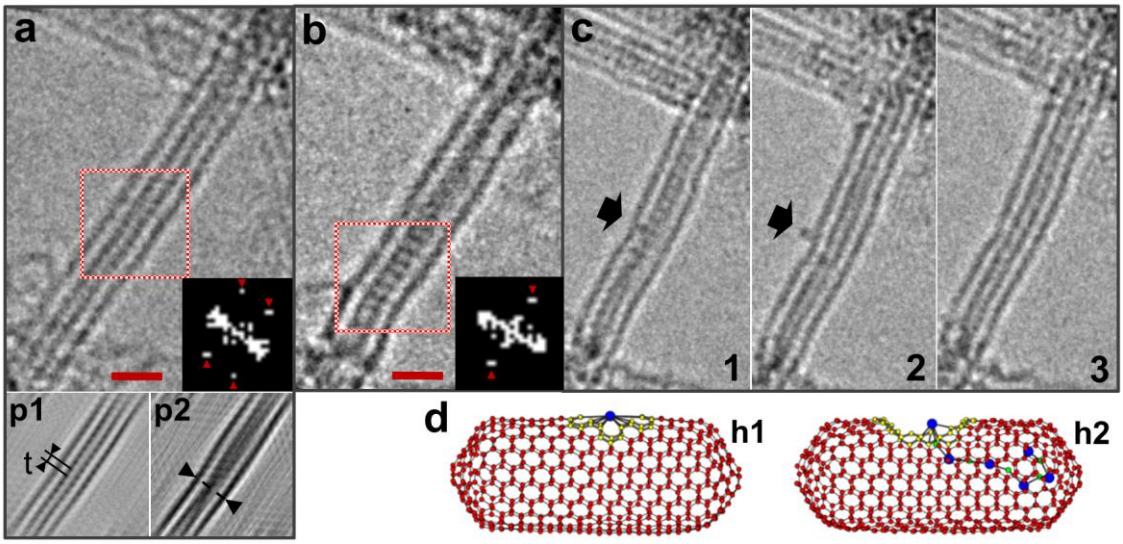

Figure 2 Iodine nanoribbon configurations in a small diameter (~ 1.1 nm) SWCNT, illustrating sequential ejection and reconfiguration events. Scale bars: 1 nm. (a) Two-atomic row iodine nanoribbon, p1, with t = 0.27 nm axial periodicity, ~0.31 nm inter-row spacing from FFT. Twisted configuration, p2. Small panels: FFT filtered images. (b) Metastable ladder-type structure, with t = 0.28 nm axial periodicity from FFT. (c) Key events of dynamic process, snapshots from movie (ESM-2). Panel 1: ejection site indicated by arrow; atom from nanoribbon penetrates inter-wall spacing; Panel 2: atom traverses nanotube wall and remains in proximity to outside wall; Panel 3: after atom ejection, iodine nanoribbon reconfigures with high regularity. (d) MD simulations illustrating "plugging" of side holes with iodine atoms, for 12 atom- (h1) and 24 atom- (h2) holes, respectively. Both holes effectively block/hinder passage of other atoms through the ejection site.

Figure 2(a) shows HRTEM images of the iodine nanoribbon before any side defects that would allow iodine release are generated. Images were taken under an electron beam dose of 0.4 A/cm^2 and illustrate the appearance of the ribbon as it moves under the beam between untwisted (p1) and twisted (p2) configurations. This (and the accompanying distortion of the nanotube in p2) is characteristic of this iodine polytype [14]. Identification of structure from Figure 2 as being iodine-only was based on the similarity with the iodine ribbon like-structures published in Ref. [14], and the clear incompatibility of the observed inter-atomic distances with any ribbon-like, bi-atomic AgI phases predicted to exist by MD and DFT simulations (supported by previous work [19] as well as our own simulations; see also ESM-1).

By increasing the electron beam dose to 2 A/cm^2, a defective region (visible as a kink indicated by arrow in Figure 2(c)) is induced in the side-wall of the nanotube, leading to ejection of the filling through the nanotube side. HRTEM was able to image single iodine atoms (see Methods) while in various metastable states of this process, i.e. states that were stable long enough to be captured with the 1 s temporal resolution of our experiment. These images are taken from a movie of the events (given in ESM-2) and shown in Figure 2(c), depicting key stages of a proposed iodine ejection scenario: 1, filling atom moves inside the van der Waals spacing between the nanoribbon and the nanotube, leading to the decrease of interatomic spacing between atom and nanotube wall to almost zero; 2, atom traverses the nanotube wall and remains in proximity to its outer side; and 3, no ejection occurs as the nanoribbon inside reconstructs. Snapshots of these stages were obtained repeatedly over the whole observation period, the movie in ESM-2 providing several cycles of them. Though HRTEM could capture only metastable states (while very fast dynamical processes, such as adatom diffusion along a perfect graphenic surface [20-21], even if they occur, are not expected to be observed in real time with the temporal resolution used here or even the highest yet achieved [22]) the proposed ejection scenario is supported by the following arguments: (i) we captured a similar number of images for stages 1 and 2, supporting the idea that they have a common

origin; on the contrary, significantly more images of "stage 2" would be recorded if additional processes, such as atomic migration along the nanotube's outer surface from unspecified external iodine pools to the kink would play a significant role in our observations. (ii) The strong reduction of the van der Waals spacing in stage 2 can be achieved only through bonding of the filling atom with the nanotube inner wall [6] making the return of the atom to the ribbon highly unlikely; a similar decrease in the van der Waals spacing was observed in the binding of an encapsulated transition metal atom to the nanotube inner surface, which was then shown to be a pathway towards tube wall breakage and atom exit (followed by a complete nanotube sectioning) [6]. These considerations permit us to correlate the three stages observed experimentally despite the 1 s temporal resolution. We also note that a similar temporal resolution has been used in inferring scenarios in a variety of dynamic processes with mixed fast and slow stages [8].

Between ejection events, the nanoribbon repair appears to be almost perfect, despite competition with further side-wall ejection events. Moreover, ejection occurs from a central portion of the ribbon, requiring atomic reorganisation to occur over an extended distance. In this aspect the process is similar to that which occurs during the filling of a nanotube with molten ionic phases, when the two crystallizing parts join and ionic bonds re-arrange themselves in a domino-like fashion [3]. Here, however, the interaction between the atoms in the nanoribbon is predominantly of van der Waals type.

3. Discussion

The intermittent nature of the ejection events could suggest that defects in the carbon nanotube wall seal periodically. Room temperature permeation [23] and ejection of hydrocarbon chains [7] through nanotube pores, followed by pore closing have been observed as single events. However, we consider it unlikely that in the same region repeated instances of destruction followed by such complex repair to a stable configuration would occur *repeatedly*, contrary to our observations. More likely, we believe, is that iodine released from the nanoribbon temporarily blocks the side hole, inhibiting the next ejection event, so that the ejection occurs sporadically. This is supported by the observation of repeated events where filling atoms are seen trapped either on the inner or outer sides of the nanotube wall in the region of the ejection site. Support for this picture comes from MD simulations (further details in ESM-1) which also permit an estimate of the size of side-wall vacancies that prevent iodine ion transfer. These consider bi-capped SWCNTs, with hole sizes corresponding to the removal of 12 or 24 C atoms (5.7 Å and 9.6 Å diameter holes respectively), and investigate the reverse passage of material, from an *external* AgI rich melt *into* a nanotube. The melt ensures the simulation contains interactions between the wall and iodine species from a dense condensed phase, whilst enhancing the collision rate compared to a crystalline or gas-like iodine-only environment, each of which would have greatly limited the likelihood of an ion-transfer event occurring during the time-scale accessible to MD. Figure 2(d) shows snapshots for the two situations taken after ~ 200 ps of MD simulation - sufficient time for AgI to enter the end of uncapped nanotubes and form multi-row encapsulated nanocrystals several nm in length in a comparative process (see ESM-1). We find that the smaller side hole (h1) becomes effectively blocked by an iodine ion that binds to the edge atoms and which prevents the passage of material across the nanotube wall. For the larger side hole (h2), only a relatively small amount of ionic material passes across, indicating the iodine ion has also blocked the hole, although less completely than for the smaller hole; this process is much slower than when material enters that nanotube through the open ends (see ESM-1). Although not directly comparable to the observed dynamical process (where the longer timescale prohibits MD simulation) these simulations support the principle of iodine "plugging'' holes in the nanotube wall, thereby inhibiting the free passage of material through it. This blocking mechanism using atoms from the filling, in this case iodine, can provide a degree of stabilization for defective SWCNTs. This phenomenon echoes a similar stabilization process based on the trapping of transition metals within vacancies of graphene sheets and multiwalled carbon nanotubes [24].

Our MD simulations also show that the nanotube

from Figure 1 must have repaired itself to at least the level of a 12-atom vacancy hole in order to stop any further sublimation of the AgI material inside, for which the I atoms constitute a probe. Following the ejection of a large nanowire section, such as in Figure 1, the end of the remaining part can be expected to play a crucial part in the repair, through the way it relaxes within the space made available in the nanotube, the modifications in the charges of the ions, and through them the associated electrostatic field within the nanotube. We have used DFT to explore these changes, choosing a section of the structure obtained in Figure 1(d) of several unit cells in length as shown in Figure 3(a). Holding the atoms fixed at one end, those at the other were permitted to relax while inside a SWCNT of 1.5 nm in diameter. Figure 3(b) shows that after relaxation both ionic species tend to approach each other at the free end, in doing so moving inwards from the side wall and lengthways along the tube. This "shearing" and accompanying decrease in diameter of the filling represents a mechanism by which the structure could accommodate the constricted, funnel region of the encapsulating nanotube that we have observed. We also find that relaxation produces a polar end, which could discriminatively attract oppositely charged, mobile ions from within the region to the right (left of Figure 1), potentially encouraging re-crystallisation in a step-by-step growth process. Electrostatic effects were investigated using Mulliken charges from DFT in a discrete dipole approximation model (DDA), previously used to describe polarization effects on the nanotubes induced by encapsulated nanocrystals [2, 25]. Calculating the electrostatic potential within the tube, we find this to be significant, fractions of an eV and well above thermal energy at room temperature (RT), over a distance exceeding 1 nm from the polar end, supporting the view that the nanowire reconfiguration across a nano-constriction can be aided by relatively long-ranged electrostatic forces generated by partially ionic fillings, as here. Note that under the beam conditions we used (100 keV and low doses, 0.4 – 2 A/cm^2), beam-induced thermal heating is not expected to occur [8], [17, 26-27]. An example potential energy map supporting the description above is given in Figure 3(c).

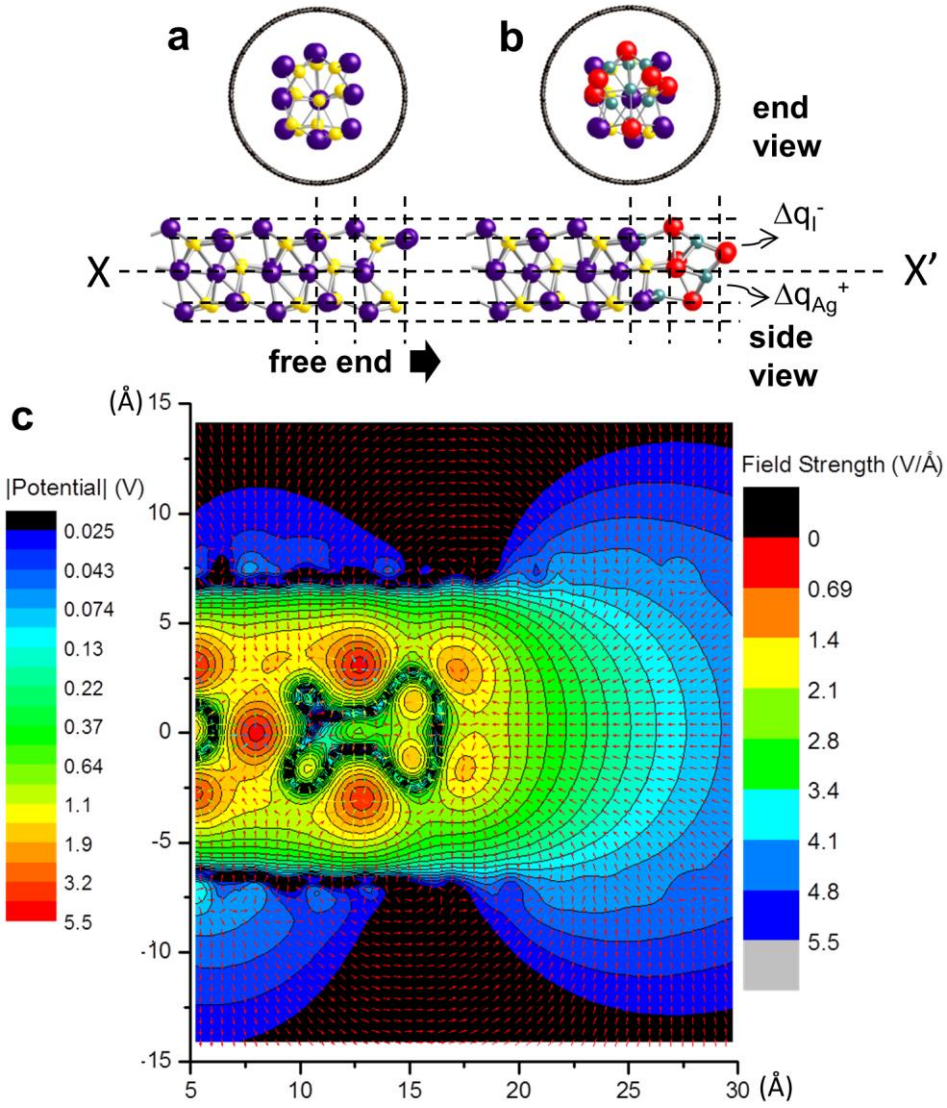

Figure 3 Relaxation of free end of the AgI structural model: (a) before, and (b), after relaxation. Atoms that showed significant relaxation: I-red, Ag- green; for the rest: I-purple, Ag-yellow. At the polar end (b) I^- ions gain $\Delta q_I^- \cong +0.3$ e, while Ag^+ ions lose $\Delta q_{Ag}^+ \cong -0.1$ e compared to (a). (c) Potential energy map corresponding to the broken nanowire from Figure 3(b) illustrating that electrostatic effects in excess of the thermal energy (25 meV) extend beyond 1 nm from the polar end of the crystal. Cross section taken through the plane X-X' passing through the nanotube's long axis and perpendicular to the view plane. Direction and magnitude of the field lines are symbolized by arrows. The minimum value for the potential scale corresponds to thermal energy at RT.

4. Conclusions

In conclusion, we have observed dynamic processes in the confining environment of SWCNTs filled with inorganic nanowires that reveal mechanisms that favour the repair of the encapsulated nanowires and increase the stability of damaged nanotubes. A nanowire of partially ionic AgI is observed to regain continuity following the ejection of several sub-units, aided by relaxation processes within the nanowire and sufficiently long-ranged electrostatic forces which encourage the restorative migration of charged species to the fractured end. Atom-by-atom, sequential release from a central portion of an iodine nanoribbon is accompanied by small scale reorganizations over an extended distance that result in repeated restoration of nanoribbon integrity. Our observations also show that certain encapsulated compounds can help *stabilize* single walled carbon nanotubes under beam exposure, providing species that can bind to multivacancies created in the sidewalls - this contrasts with known cases where

fillings (e.g. oxygen-rich or transition metals) have accelerated both degradation and disintegration, or nanotube sectioning and closing. These principles contribute towards establishing a blueprint for the design of robust and reconfigurable nanowire systems. Finally, we envisage that a detailed understanding of the underlying processes will also enable their exploitation in the controlled formation of intra-tube nanowire heterojunctions.

5. Methods and Computational Details

5.1 HRTEM: Choice of imaging/irradiation conditions and effects on materials. Imaging and Simulation

HRTEM was performed at room temperature with a JEOL 3000 F field-emission gun microscope operated at 100 keV and electron beam doses from 0.4 to 2 A/cm^2. This energy is slightly above the knock-on threshold of ~ 86 keV for carbon atoms in pure carbon nanostructures [15, 17], such as empty SWCNTs, and is considered as appropriate for routine imaging of such nanostructures [15]. We are also aware that the knock-on threshold can be lowered by an undetermined degree by the presence of impurities [12] or, in our case, filling material. In these circumstances, we chose 100 keV in order to ensure that we could induce changes to the nanotubes as the starting points for the processes involving the inorganic nanowires, but we deliberately kept the doses orders of magnitude lower than values used in other works [16] in order to reduce the rate of knock-on displacement of carbon atoms [9],[17]. Indeed, calculations based on Ref. [17] show that at 100 keV, under beam current densities of 0.4 to 2 A/cm^2, with a threshold energy for carbon knock on of ~ 17eV [15], the displacement rate of carbon atoms p ranges between 3.6 x 10^{-5} to 1.8 x 10^{-4} s^{-1}; this is equivalent to saying that each carbon atom under the beam has been displaced *once* in $1/p$ ranging from 28000 s (for the lowest dose), to 5600 s (for the highest dose), respectively. These values compare well with our observations times, which we kept ~ tens of minutes for the lowest doses, and several minutes for the highest dose. This choice of doses is also supported by the many observations of AgI filled nanotubes we made, where no degradation of either nanotube or filling was noted during routine observations or acquisition of focal series. In general, our experiments proceeded by examining the structures at the lowest doses, and then carefully increasing the dose until changes were recorded.

We also considered other possible effects of the e-beam on the observed structures. Based on Ref. [17, 26] thermal heating of the SWCNTs induced by the electron beam is considered to be negligible. Other potential e-beam induced effects involve the encapsulated inorganic nanowires. Knock-on of any of the heavier Ag or I atoms has a highly reduced rate compared to the carbon knock-on, and can be neglected [17]. Ref. [16, 28] showed that ionic silver halides, such as AgCl and AgBr, encapsulated within SWCNTs can be reduced to crystalline Ag under intense e-beam irradiation. However, AgBr nanowires inside SWCNTs could only be reduced to Ag at ~ 72 A/cm^2 and 120 keV (corresponding to a displacement rate p of ~ 0.008 s^{-1}, $1/p$ ~ 121 s, i.e. rates that are orders of magnitude larger than in our case) and only after locally damaging the protective SWCNT cage, and only in that specific region [16]. AgI is expected to have a lower propensity for reduction, as I is the largest (stable) halogen atom and would diffuse to the exit point with more difficulty. Supported also by our own observations on both AgI@SWCNTs and extraneous (un-encapsulated) AgI nanocrystals (occasionally seen in our sample), which did not show crystallographic changes upon exposure in the conditions we describe, we determined that the doses we used did not reduce AgI to Ag. The AgI@SWCNT structure from Figure 1 panel 1 was examined over tens of minutes with doses between 0.4 and 1 A/cm^2 without observing any structural evolution of the nanotube and encapsulated nanowire, and just minor and gradual build-up of e-beam induced contamination on the borders of the region observed (see ESM-1). The same crystallization phase was observed several times within our sample. A low dose of 0.4 A/cm^2 was used to establish the initial structure of the iodine nanoribbon from Figure 2 (a) (as low stability was expected for the narrow SWCNT that encapsulated it) resulting in images with somewhat lower S/N ratio. Dose was then ramped to 2 A/cm^2 to induce

structural evolution in both structures. Identification of structures from Figure 1 and 2 as being AgI and iodine, respectively, is supported by EDX, our prior work [2] and other literature [14, 19] (ESM-1).

The microscope has a spherical aberration coefficient (C_s) of 0.57mm giving a point resolution of ~ 0.225 nm at 100 keV, as obtained by optimizing the contrast transfer function as in Ref. [9] (see ESM-1 for an example of achieved resolution). This spatial resolution is very similar to that in Ref. [9], where 120 keV HRTEM *without aberration correction* was used to provide direct evidence of atomic defects in graphene layers and SWCNTs. This resolution figure is better than the dimensions encountered within our AgI and I nanowires, whose evolution is our focus: the ionic radius of single I ions is ~ 0.2 nm, so single I ions can be resolved, while various crystal periodicities that need to be resolved are larger than the spatial resolution (as well as being larger than the inter-chain distances of carbon atoms within the nanotube/graphene lattice, resolved in Ref. [9] without an aberration corrector). Image resolution is 1024 × 1024 pixels. A low pass convolution filter with a 5 × 5 kernel was applied for Figure 1 of main text, and Figures S1, S3, and S5 in ESM-1. The rest of the images presented were unfiltered.

Focal series and exit wavefunction reconstruction were performed for the structure in Figure 1 (see ESM-1). Structural models were generated with Crystal Maker [29] and modified through DFT to match the exit plane wavefunction reconstructed image (done with JEMS) [30], while their image simulations (with SimulaTEM) [31] were compared with the sets of focal series (in ESM-1).

The movie in Electronic Supplementary Material ESM-2 shows sequential ejection /reorganization of the iodine nanoribbon and was obtained by collating 40 consecutive frames. HRTEM simulations of vacancies plugged by one iodine atom are compatible with experimental images such as that shown in Panel 2 of Figure 2(c).

5.2. DFT Ab Initio Calculations (Further Details in Supporting Information)

First-principles calculations used to investigate the stability of candidate structures for the AgI phase observed in HRTEM images were performed using the plane-wave pseudopotential code CASTEP [32]. We used ultrasoft pseudopotentials, plane wave cut-offs up to 350 eV and k-point sampling with $\Delta k<0.05$ Å^{-1}, with structures relaxed till residual forces fell below 0.02 eV Å^{-1}. We used the Perdew-Burke-Ernzerhof form of the generalized gradient approximation [33] to the exchange-correlation interaction of density functional theory. These predict the wurtzite phase of AgI as most stable, with lattice parameters a=4.67 Å and c=7.66 Å, in good agreement with the experimental values of 4.60 Å and 7.52 Å respectively [34]. The lattice parameter of planar monolayer graphene is predicted to be a=2.463 Å, also in good agreement with the experimental value of 2.461 Å.

Model encapsulated nanocrystal systems were constructed working within the dual constraints of experimentally-determined dimensions and available computational resources. On the basis of the tube diameter (d_{CNT}) determined from the analysis of HRTEM images we focused on (n,m) nanotubes: (17,0), d_{CNT}=1.33 nm, t=4.26 Å (fundamental repeat length); (18,0), d_{CNT}=1.41 nm, t=4.26 Å; and (15,5), d_{CNT}=1.41 nm, t=15.36 Å. The CASTEP code models an overall periodic structure, and so to model the combined nanotube+filling we constructed commensurate approximants with unit cells containing either 2 or 4 basic repeat units of (17,0) and (18,0), and 1 or 2 basic repeat units of (15,5), corresponding to up to 520 C atoms. AgI fillings were introduced, initially based upon cuts of bulk wurtzite and zincblende AgI, with atomic coordinates compressed or expanded in an axial direction to be commensurate with the nanotubes, and stay close to the axial periodicity of t ~0.78 nm for the AgI filling, as determined from HRTEM. The nanotube+filling structures were periodically repeated with tube-tube separations of 6 or 8 Å. Both HRTEM simulations and simple estimates based upon atomic/Van der Waals dimensions pointed to a triple-row arrangement of I atoms, and so other candidate structures were considered comprising of 2x3, 3x3, and 1+3+1 and 2+3+2 rows of AgI atoms, which were each permitted to relax.

The structure in Figure 1 was obtained within an (18,0) SWCNT, and resulted in the closest match with experiment when simulating HRTEM images

(shown in Figure S1 of ESM-1). It was obtained by relaxing a cut from bulk zincblende AgI with the [-1,-1,2] direction along the nanowire's long axis. A closely related configuration was also obtained within a (15,5) SWCNT (Figure S8 in ESM-1). A discussion concerning the possibility of formation of inorganic nanotubes and irregular nanowires (as previously predicted by several Molecular Dynamics calculations) [3, 19] is included in ESM-1.

5.3 Molecular Dynamics Calculations

Molecular dynamics simulations were performed to investigate the passage of ions through defective nanotube walls. In the experiments ions originate from an encapsulated nanocrystal, and are observed to pass through and away from the nanotube intermittently, on a timescale of seconds. This precludes the use of MD to study this actual process. Instead, to gain insight, we have considered the passage of ions through vacancy defects in nanotubes from a liquid AgI melt surrounding the nanotube.

We used periodic simulation cells containing 1450-1600 AgI ions surrounding 2 nm long nanotubes of up to 580 atoms. AgI, carbon-carbon and ion carbon interactions were modelled using respectively the RVP potential [35], Tersoff-II potential [36] and a fitted Lennard-Jones potential [3]. Further details about the theoretical computations are given in ESM-1.

The approach used is similar to that previously used to model SWCNT filling from melt [3]. A cylindrical volume corresponding to the SWCNT section is removed from an equilibrated liquid configuration, and replaced with a SWCNT of chosen morphology, i.e. ~ 2 nm lengths of open-ended (n,n) SWCNTs with n=8,9, and 10, or a (10,10) SWCNT capped at each end by a C_{82} hemisphere. Further MD steps are performed for ~100 ps, with the open ends of SWCNTs sealed with sections of graphene sheet to prevent filling during this stage. Once equilibrium is re-attained, these caps are then removed and/or holes created in the SWCNT sidewall by removing a set number of atoms, and MD performed for a few hundred ps at T=550 K, corresponding to just above the AgI melting point according to the AgI pair-potential model that we employ. After equilibrating systems for 100 ps at T=550 K, ions were allowed to penetrate ideal or defective nanotube structures, and systems followed for a further 200 ps. Simulations were repeated using several different initial ion configurations to assess statistical significance. Holes that we have considered correspond to 12 and 24 carbon atoms, and have radii of 0.57 and 0.96 nm respectively.

Further details regarding the comparison of time scales for ion passage through side-wall holes of capped nanotubes as opposed to passage through open-ended nanotubes without side-wall defects is given in ESM-1.

Acknowledgements

This work is supported by grants EP/G001707/1 and EP/F01919X/1 from the United Kingdom Engineering and Physical Sciences Research Council.

Electronic Supplementary Material: Supplementary Material ESM-1: HRTEM - focal series, exit wave reconstruction, and image simulations of AgI structural models, EDX, wider region with AgI@SWCNT structure before and after nanowire section ejection, and justification of spatial resolution achieved at 100 keV; DFT simulations of AgI nanowire configurations inside SWCNTs and associated Mulliken charges; MD simulations of ion transfer through defective nanotube walls. Supplementary Material ESM-2: Movie showing multiple and successive atom release from iodine ribbon through side hole in the nanotube and restoration events within the ribbon. ESM-1 and ESM-2 are available in the online version of this article at http://dx.doi.org/10.1007/s12274-012-0267-5.

References

[1] Meyer, R. R.; Sloan, J.; Dunin-Borkowski, R. E.; Kirkland, A. I.; Novotny, M. C.; Bailey, S. R.; Hutchison, J. L.; Green, M. L. H. Discrete Atom Imaging of One-Dimensional Crystals Formed within Single-Walled Carbon Nanotubes. *Science* **2000,** *289*, 1324-1326.

[2] Ilie, A.; Bendall, J. S.; Nagaoka, K.; Egger, S.; Nakayama, T.; Crampin, S. Encapsulated Inorganic Nanostructures: A

Route to Sizable Modulated, Noncovalent, on-Tube Potentials in Carbon Nanotubes. *ACS Nano* **2011,** *5*, 2559-2569.

[3] Bishop, C. L.; Wilson, M. The Filling of Flexible Carbon Nanotubes by Molten Salts. *J. Mater. Chem.* **2009,** *19*, 2929-2939.

[4] Chamberlain, T. W.; Meyer, J. C.; Biskupek, J.; Leschner, J.; Santana, A.; Besley, N. A.; Bichoutskaia, E.; Kaiser, U.; Khlobystov, A. N. Reactions of the Inner Surface of Carbon Nanotubes and Nanoprotrusion Processes Imaged at the Atomic Scale. *Nat. Chem.* **2011,** *3*, 732-737.

[5] Chen, W.; Pan, X. L.; Willinger, M. G.; Su, D. S.; Bao, X. H. Facile Autoreduction of Iron Oxide/Carbon Nanotube Encapsulates. *J. Am. Chem. Soc.* **2006,** *128*, 3136-3137.

[6] Zoberbier, T.; Chamberlain, T. W.; Biskupek, J.; Kuganathan, N.; Eyhusen, S.; Bichoutskaia, E.; Kaiser, U.; Khlobystov, A. N. Interactions and Reactions of Transition Metal Clusters with the Interior of Single-Walled Carbon Nanotubes Imaged at the Atomic Scale. *J. Am. Chem. Soc.* **2012,** *134*, 3073-3079.

[7] Borrnert, F.; Gorantla, S.; Bachmatiuk, A.; Warner, J. H.; Ibrahim, I.; Thomas, J.; Gemming, T.; Eckert, J.; Cuniberti, G.; Buchner, B., et al. In Situ Observations of Self-Repairing Single-Walled Carbon Nanotubes. *Phys. Rev. B.* **2010,** *81*.

[8] Suenaga, K.; Wakabayashi, H.; Koshino, M.; Sato, Y.; Urita, K.; Iijima, S. Imaging Active Topological Defects in Carbon Nanotubes. *Nat. Nanotechnol.* **2007,** *2*, 358-360.

[9] Hashimoto, A.; Suenaga, K.; Gloter, A.; Urita, K.; Iijima, S. Direct Evidence for Atomic Defects in Graphene Layers. *Nature* **2004,** *430*, 870-873.

[10] Ding, F.; Jiao, K.; Wu, M. Q.; Yakobson, B. I. Pseudoclimb and Dislocation Dynamics in Superplastic Nanotubes. *Phys. Rev. Lett.* **2007,** *98*.

[11] Kotakoski, J.; Krasheninnikov, A. V.; Nordlund, K. Energetics, Structure, and Long-Range Interaction of Vacancy-Type Defects in Carbon Nanotubes: Atomistic Simulations. *Phys. Rev. B.* **2006,** *74*.

[12] Warner, J. H.; Schaffel, F.; Zhong, G. F.; Rummeli, M. H.; Buchner, B.; Robertson, J.; Briggs, G. A. D. Investigating the Diameter-Dependent Stability of Single-Walled Carbon Nanotubes. *ACS Nano* **2009,** *3*, 1557-1563.

[13] Bendall, J. S.; Ilie, A.; Welland, M. E.; Sloan, J.; Green, M. L. H. Thermal Stability and Reactivity of Metal Halide Filled Single-Walled Carbon Nanotubes. *J. Phys. Chem. B* **2006,** *110*, 6569-6573.

[14] Guan, L. H.; Suenaga, K.; Shi, Z. J.; Gu, Z. N.; Iijima, S. Polymorphic Structures of Iodine and Their Phase Transition in Confined Nanospace. *Nano Lett.* **2007,** *7*, 1532-1535.

[15] Smith, B. W.; Luzzi, D. E. Electron Irradiation Effects in Single Wall Carbon Nanotubes. *J. Appl. Phys.* **2001,** *90*, 3509-3515.

[16] Kobayashi, K.; Suenaga, K.; Saito, T.; Shinohara, H.; Iijima, S. Photoreactivity Preservation of Agbr Nanowires in Confined Nanospaces. *Adv. Mater.* **2010,** *22*, 3156.

[17] Banhart, F. Irradiation Effects in Carbon Nanostructures. *Rep. Prog. Phys.* **1999,** *62*, 1181-1221.

[18] Costa, P. M. F. J.; Golberg, D.; Mitome, M.; Hampel, S.; Leonhardt, A.; Buchner, B.; Bando, Y. Stepwise Current-Driven Release of Attogram Quantities of Copper Iodide Encapsulated in Carbon Nanotubes. *Nano Lett.* **2008,** *8*, 3120-3125.

[19] Baldoni, M.; Leoni, S.; Sgamellotti, A.; Seifert, G.; Mercuri, F. Formation, Structure, and Polymorphism of Novel Lowest-Dimensional Agl Nanoaggregates by Encapsulation in Carbon Nanotubes. *Small* **2007,** *3*, 1730-1734.

[20] Gan, Y. J.; Sun, L. T.; Banhart, F. One- and Two-Dimensional Diffusion of Metal Atoms in Graphene. *Small* **2008,** *4*, 587-591.

[21] Krasheninnikov, A. V.; Lehtinen, P. O.; Foster, A. S.; Pyykko, P.; Nieminen, R. M. Embedding Transition-Metal Atoms in Graphene: Structure, Bonding, and Magnetism. *Phys. Rev. Lett.* **2009,** *102*.

[22] Warner, J. H.; Ito, Y.; Rummeli, M. H.; Buchner, B.; Shinohara, H.; Briggs, G. A. D. Capturing the Motion of Molecular Nanomaterials Encapsulated within Carbon Nanotubes with Ultrahigh Temporal Resolution. *ACS Nano* **2009,** *3*, 3037-3044.

[23] Koshino, M.; Solin, N.; Tanaka, T.; Isobe, H.; Nakamura, E. Imaging the Passage of a Single Hydrocarbon Chain through a Nanopore. *Nat. Nanotechnol.* **2008,** *3*, 595-597.

[24] Rodriguez-Manzo, J. A.; Cretu, O.; Banhart, F. Trapping of Metal Atoms in Vacancies of Carbon Nanotubes and Graphene. *ACS Nano* **2010,** *4*, 3422-3428.

[25] Ilie, A.; Egger, S.; Friedrichs, S.; Kang, D. J.; Green, M. L. H. Correlated Transport and High Resolution Transmission Electron Microscopy Investigations on Inorganic-Filled Single-Walled Carbon Nanotubes Showing Negative Differential Resistance. *Appl. Phys. Lett.* **2007,** *91*.

[26] Zobelli, A.; Gloter, A.; Ewels, C. P.; Colliex, C. Shaping Single Walled Nanotubes with an Electron Beam. *Phys. Rev. B.* **2008,** *77*.

[27] Rodriguez-Manzo, J. A.; Banhart, F. Creation of Individual Vacancies in Carbon Nanotubes by Using an Electron Beam of 1 Angstrom Diameter. *Nano Lett.* **2009,** *9*, 2285-2289.

[28] Sloan, J.; Wright, D. M.; Woo, H. G.; Bailey, S.; Brown, G.; York, A. P. E.; Coleman, K. S.; Hutchison, J. L.; Green, M. L. H. Capillarity and Silver Nanowire Formation Observed in Single Walled Carbon Nanotubes. *Chem. Commun.* **1999**, 699-700.

[29] *Crystalmaker*, 2.0; CrystalMaker Software: Oxford, 2006.

[30] Stadelmann, P. *Jems*, Interdisciplinary Centre for Electron Microscopy: EPFL, 2010.

[31] Gomez-Rodriguez, A.; Beltran-del-Rio, L. M.; Herrera-Becerra, R. Simulatem: Multislice Simulations for General Objects. *Ultramicroscopy* **2010,** *110*, 95-104.

[32] Clark, S. J.; Segall, M. D.; Pickard, C. J.; Hasnip, P. J.; Probert, M. J.; Refson, K.; Payne, M. C. First Principles Methods Using Castep. *Z. Kristallogr.* **2005,** *220*, 567-570.

[33] Perdew, J. P.; Burke, K.; Ernzerhof, M. Generalized Gradient Approximation Made Simple. *Phys. Rev. Lett.* **1996,** *77*, 3865-3868.

[34] Hull, S.; Keen, D. A. Pressure-Induced Phase Transitions in Agcl, Agbr, and Agi. *Phys. Rev. B.* **1999,** *59*, 750-761.

[35] Parrinello, M.; Rahman, A.; Vashishta, P. Structural Transitions in Superionic Conductors. *Phys. Rev. Lett.* **1983,** *50*, 1073-1076.

[36] Tersoff, J. New Empirical-Approach for the Structure and Energy of Covalent Systems. *Phys. Rev. B.* **1988,** *37*, 6991-7000.